Remote Sensing of Environment 236 (2020) 111420

Contents lists available at ScienceDirect

Remote Sensing of Environment

journal homepage: www.elsevier.com/locate/rse

Solar-induced chlorophyll fluorescence and its link to canopy photosynthesis in maize from continuous ground measurements

Zhaohui Li[a,b,c,1], Qian Zhang[a,b,c,1], Ji Li[a], Xi Yang[d], Yunfei Wu[a], Zhaoying Zhang[a], Songhan Wang[a], Hezhou Wang[e], Yongguang Zhang[a,b,c,*]

[a] International Institute for Earth System Sciences, Nanjing University, Nanjing, 210023, China
[b] Jiangsu Provincial Key Laboratory of Geographic Information Technology, Nanjing University, Nanjing, 210023, China
[c] Collaborative Innovation Center of Novel Software Technology and Industrialization, Nanjing, 210023, China
[d] Department of Environmental Sciences, University of Virginia, Charlottesville, VA, USA
[e] Farmland Irrigation Research Institute of Chinese Academy of Agricultural Sciences, Xinxiang, Henan, China

ARTICLE INFO

Keywords:
Solar-induced chlorophyll fluorescence
GPP
Plant growth stage
Canopy structure
SIF_{yield}
LUE
Environmental conditions

ABSTRACT

Remote sensing of solar-induced chlorophyll fluorescence (SIF) provides great potential for estimating gross primary production (GPP) of terrestrial ecosystems. A strong relationship between SIF and GPP has been observed at the seasonal scale from both ground-based and satellite observations. However, variations of SIF due to changes in plant growth stages appear to influence the SIF-GPP relationship. It remains unclear how this relationship is affected by plant growth-related changes, especially for C4 plants such as maize. In this study, continuous *in situ* measurements for canopy far-red SIF retrieval and GPP calculation were made in maize during the growing season of 2017. Diurnal and seasonal variations of canopy SIF and its yield (SIF_{yield}) were analyzed over different growth stages of maize to understand how they affect the relationship with GPP. The results show that the relationship between SIF and GPP varies with the growth stages of maize during the growing season, indicating that canopy structure has a strong impact on the seasonal variations of canopy SIF and its relation to GPP. Furthermore, we found that SIF_{yield} is significantly correlated with canopy photosynthetic light use efficiency (LUE) at the canopy level throughout the season. However, it is almost uncorrelated with LUE after adjusting for the effects of canopy structure with the structural vegetation index MTVI2. This finding highlights the importance of canopy structure in the relationship between SIF_{yield} and LUE, complicating the use of canopy SIF for tracking vegetation physiological activity. Overall, our observation-based findings show that canopy structure affects the SIF-GPP relationship, strengthening our understanding of the mechanistic link between SIF and photosynthesis.

1. Introduction

Terrestrial gross primary production (GPP) is an important variable for exploring and quantifying carbon fixation by terrestrial ecosystems. However, direct measurements of GPP at landscape or regional scale are still challenging. A state-of-the-art method of GPP estimation is the eddy covariance (EC) technique. However, EC can only measure carbon fluxes associated with a small footprint area, typically in the order of ~1 km^2, depending on the setup of EC towers and aerodynamic properties (Kljun et al., 2004; Chen et al., 2009; Damm et al., 2010). The light-use-efficiency (LUE) model (Monteith, 1972), which uses data from EC towers and vegetation indices (VIs) calculated from satellite data, has been used to estimate GPP at larger scales (Field et al., 1995; Ryu et al., 2011; Zhao et al., 2005). However, estimating photosynthetic LUE and absorbed photosynthetically active radiation (APAR) over large scales is still challenging owing to their variation with different ecosystems, physiological factors, and environmental conditions (Frankenberg et al., 2011; Medlyn, 1998).

Solar-induced chlorophyll fluorescence (SIF) is a radiation flux driven by APAR, emitted as a light in the spectral range of ~650–~800 nm. It is intrinsically linked to plant photosynthesis and is considered as a potential indicator of photosynthetic activity in remote sensing applications (Porcar Castell et al., 2014; Rascher et al., 2015; Goulas et al., 2017). Retrievals of SIF with various remote sensing techniques and platforms have provided a novel method of estimating GPP. Recently, the development of observations of SIF based on

* Corresponding author. International Institute for Earth System Sciences, Nanjing University, Nanjing, 210023, China.
E-mail address: yongguang_zhang@nju.edu.cn (Y. Zhang).
[1] Z.L. and Q.Z. contributed equally to this work.

https://doi.org/10.1016/j.rse.2019.111420
Received 30 November 2018; Received in revised form 11 August 2019; Accepted 12 September 2019

spaceborne and airborne technologies has shown the potential of using SIF for GPP modeling at large spatial scales (Damm et al., 2014; Frankenberg et al., 2011, 2012; 2014; Guanter et al., 2014; Joiner et al., 2011, 2013; Qiu et al., 2018; Rascher et al., 2015; Verma et al., 2017; Zarco-Tejada et al., 2009). For example, Frankenberg et al. (2011) and Guanter et al. (2012) investigated the relationship of SIF-GPP based on the data from Greenhouse gases Observing SATellite (GOSAT) and found a strong linear correlation between SIF and GPP.

However, most studies based on spaceborne and airborne technologies ignore canopy structure effects on the relationship between SIF and GPP. The coarse spatial and temporal resolution of satellite retrieved SIF will also complicate the analysis of structural effects. *In-situ* spectral measurement techniques have recently emerged, which provide the advantage of continuous, reliable measurements (e.g. reduced atmospheric influence). These measurements allow us to explore the relationship between SIF and GPP at finer spatial and temporal scales (Cogliati et al., 2015; Daumard et al., 2010; Drolet et al., 2014; Miao et al., 2018; Yang et al., 2015, 2018a). Recently, both modeling and observations studies have indicated that canopy structure exerts a strong influence on SIF signals (Du et al., 2017; Liu et al., 2018; Migliavacca et al., 2017; Yang et al., 2018b). For instance, Yang et al. (2018b) examined the effects of crops canopy structure on SIF based on data collected through an airborne platform, showing that over 76% of the variation in SIF among different crop types was related to variations in plant biochemistry (e.g. leaf pigments, water and dry matter) and structure. Hence, further studies are needed to improve our understanding of how canopy structure impacts the SIF-GPP relationship.

Generally, the link between SIF and GPP is studied by assuming that SIF contains information regarding both APAR and LUE (Guanter et al., 2014; Porcar-Castell et al., 2014; Rascher et al., 2015; Wieneke et al., 2016;). Ground-based measurements have shown strong SIF-APAR and GPP-APAR relationships as well as a significant correlation between SIF yield (SIF_{yield} = SIF/APAR) and LUE (Yang et al., 2015, 2018a). However, the identification of structural effects on SIF signals has recently led to a debate on whether the relationship between SIF and GPP is driven by APAR only or by both APAR and LUE (Du et al., 2017; Miao et al., 2018; Li et al., 2018; Wieneke et al., 2018; Zhang et al., 2018a). Wieneke et al. (2018) found that SIF_{yield} is affected by seasonal changes in canopy structure, but that a strong correlation between diurnal LUE and SIF_{yield} is still present after correcting for seasonal structural effects, though the correlation is not obvious in half-hourly data. Therefore, how canopy structure influences SIF-GPP, and SIF_{yield}-LUE relationships remains unclear. Is canopy structure one of the determinants of the strong SIF-GPP relationship? To what extend can SIF_{yield} explain LUE after compensating for canopy structure effects?

Studies on the SIF-GPP relationship at different plant growth stages are limited, in particular for C4 plants. C4 photosynthesis has evolved from the C3 photosynthetic pathway. C4 plants have higher material-use efficiencies and potential productivity due to greater adaptation to high light intensity, temperature and water stress than C3 plants (Sage and Monson, 1999; Still et al., 2003; Gowik and Westhoff, 2011; Sage and Zhu, 2011; Lara and Andreo, 2011). With higher potential productivity and environmental adaptation capacity, some C4 plants (e.g. maize and sugarcane) are important food and commercial crops. Maize, a typical example of C4 plant, shows large variations in canopy structure (e.g. LAI and leaf angle inclination) as plants transition through growth stage. The LAI and the leaf angle inclination of maize determine the radiative transfer of light in the canopy (Espana et al., 1999; Stewart et al., 2003), which causes a noticeable change in canopy SIF. Hence, it is necessary to investigate the canopy-scale SIF-GPP relationships for maize across different plant growth stages.

In this study, we have collected continuous ground observations of far-red SIF, hyperspectral reflectance, and gas flux exchange from EC to quantify variations in SIF and their relationship with GPP at multiple time scales (especially at sub-seasonal scales) in a maize field. The study was conducted across the entire growing season of 2017. Our major objectives were: (i) to evaluate the potential of far-red SIF for tracking the diurnal and seasonal variations of GPP and APAR for maize, (ii) to investigate the effects of canopy structure on SIF_{yield} and LUE, as well as on the canopy SIF-GPP relationship.

2. Materials and methods

2.1. Experimental site

Ground measurements were conducted in 2017 in an irrigated maize field located in Henan Province, China (34.5199 N, 115.5916 E, and about 55 m above sea elevation). The cropping regime at the site was dominated by summer maize (*Zea mays*)-winter wheat (*Triticum asetivum*) rotations. Mean annual air temperature and annual precipitation were approximately 14 °C and 704 mm, respectively. In 2017, sowing took place in late June and harvest in early October. SIF observations were collected from July 11th to November 15th, covering the vegetative, reproductive, and ripening stages of the crop.

2.2. Spectrum measurements

A FluoSpec2 system (Yang et al., 2015, 2018c) was installed to retrieve canopy SIF and several VIs. FluoSpec2 includes two spectrometers: QEPRO (signal-to-noise ratio (SNR) of 1000, range of wavelength 730–785 nm, spectral sampling interval of 0.07 nm, the full width half maximum (FWHM) of 0.17 nm, Ocean Optics, Dunedin, FL, USA) was used for SIF retrievals at the O_2-A band; HR2000+ (SNR of 250, range of wavelength 350–1100 nm, spectral sampling interval of 0.5 nm, FWHM of 1.1 nm, Ocean Optics, USA) was used for measuring canopy reflectance for the calculation of VI. Detailed information on the FluoSpec2 system can be found in Yang et al. (2018c). The fiber was mounted ~10 m above the maize canopy, and the footprint was a circle with ~ 4.4 m diameter. Atmospheric correction was performed to acquire the top-of-canopy (TOC) SIF according to the method described in Liu et al. (2019). Fibers used in this system were all produced by Ocean Optics, with 1000 μm core diameter. Calibrations of irradiance and radiance were done using a tungsten halogen light source (HL-CAL-2000, Ocean Optics, USA) and a standard reference panel (Spectralon, Labsphere, NH, USA) at noon in clear sky conditions.

A sandwich-method was used to reduce the influence of meteorological conditions (e.g. clouds) on the measurements. The spectrometer first collected solar irradiance (Eg1), then the shutter immediately switched to measure canopy radiance (Ls), and then the shutter switched back to collect solar irradiance (Eg2) immediately again (Fig. 1). All measurements were simultaneously recorded along with dark current, which was used for dark-current correction. This represented one measurement cycle, which took about 2 min. If there

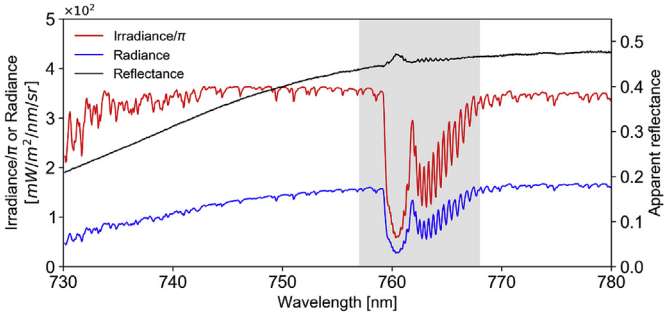

Fig. 1. Irradiance, radiance and apparent reflectance acquired within a single sandwich-measurement circle of FluoSpec2 system at about 11:30 am, July 25th, 2017. Irradiance was calculated as (Eg1 + Eg2)/2, and apparent reflectance was calculated as Radiance × π/Irradiance. The spectra range within the grayed shadow (757–768 nm) covering the oxygen absorption band (O_2-A, centered around 760 nm) was used for SIF retrieval.

was an apparent difference between Eg1 and Eg2 caused by clouds (e.g. Eg1 was measured without clouds blocking the sun while Eg2 was measured with clouds blocking the sun, or vice versa), then this set of data were dropped. A special data collection program was designed for this method. Optimizing the integral time was done automatically before each spectrum measurement in order to avoid signal saturation and guarantee sufficient SNR. The two spectrometers, four inline shutters, and one computer were enclosed in a temperature controlled box with corresponding power supply. Data quality control was conducted before subsequent analysis (Cogliati et al., 2015). The quality control criteria and corresponding thresholds used were: 1) solar zenith angles (SZA) $>$ 60°, 2) digital counts $<$ 200000, 3) $|Eg1 - Eg2| \times 100 \div Eg1 < 0.1$, 4) apparent reflectance $<$ 1, 5) digital counts÷dark current $>$ 30.

2.3. Measurements of CO_2 fluxes and meteorological data

The EC technique (Baldocchi et al., 1988, 1997) was used to measure CO_2 fluxes. An EC flux system was installed in the southeast direction at ~4 m height, about 500 m away from the FluoSpec2 system, and was covered by the same maize and soil types. The FluoSpec2 system was installed within the major wind direction of the EC flux tower. The 10 Hz raw ecosystem flux data were processed using EddyPro software (version 6.1.0, LI-COR, USA), and were then quality controlled. GPP was estimated by partitioning the daytime net ecosystem CO_2 exchange into GPP and ecosystem respiration according to Reichstein et al. (2005).

Environmental and meteorological data were continuously collected and processed every half an hour, including air temperature (Ta, HMP155, Vaisala Group, Helsinki, Finland), relative humidity (RH, HMP155, Vaisala Group, Helsinki, Finland), volumetric soil water content (SWC, Stevens Hydra Probe II, Stevens Water Monitoring Systems, Portland, USA), and total incident PAR above the canopy (PAR, LI-190SL, LI-COR Inc., Lincoln, NE, USA).

2.4. Identification of growth phases

Three growth stages were identified through *in situ* observations combined with the extended BBCH (Biologische Bundesanstalt, Bundessortenamt and Chemical industry) scale (Alcaraz et al., 2013; Lancashire et al., 1991). The BBCH growth stages of maize were grouped into three basic growth phases (Fig. 2): vegetative stage (July 11th - July 23th, from germination to panicle initiation), reproductive stage (July 24th - September 11th, from panicle initiation to start of senescence) and ripening stage (September 12th - October 10th, from senescence to harvest). Although the day of year (DOY) partition for each growth stage varies slightly, a shift of a few days would not have much influence on the results.

2.5. Data processing

2.5.1. SIF retrieval

The Spectral fitting method (SFM, Meroni and Colombo., 2006; Meroni et al., 2010; ; Mazzoni et al., 2012) was used for SIF retrievals. SFMs are based on the assumption that the spectral variations of reflectance (r) and solar-induced fluorescence (F) in the selected spectral interval can be described by a polynomial or other appropriate mathematical functions of wavelength (λ). The SFM used here assumed that both r and F were linearly related to λ. Therefore, the measured canopy radiance (Ls(λ)) can be expressed as:

$$Ls(\lambda) = \frac{r_{mod}(\lambda)E(\lambda)}{\pi} + F_{mod}(\lambda) + \varepsilon(\lambda), \quad \lambda \in [\lambda_1, \lambda_2] \tag{1}$$

where $r_{mod}(\lambda) = k_1 \times \lambda + b_1$ and $F_{mod}(\lambda) = k_2 \times \lambda + b_2$ are the linear functions. k_1, b_1, k_2, and b_2 are coefficients of the linear functions describing r and F. $E(\lambda)$ is the measured incident solar irradiance, calculated as the mean value of Eg1 and Eg2. $\varepsilon(\lambda)$ is the modeling error of observed and simulated radiance. λ_1 and λ_2 were set as 757 and 768 nm (Fig. 1), respectively. Then, SIF was quantified as a linear function of wavelength λ_m (Eq. (2)).

$$SIF = k_2 \times \lambda_m + b_2 \tag{2}$$

where λ_m is the wavelength at which incident solar irradiance reached the minimum value within the broader O_2 A oxygen absorption band around 760 nm. A SIF value was calculated about every 2 min from 8:00 am to 6:00 pm every day from July 11th to November 15th, 2017, and then the 2 min retrieved SIF were averaged every 30 min to match with the half-hourly EC flux data.

The canopy height of maize grew from ~ 1 m at the start of our study to ~ 2.5 m at the peak of the growing season. Accordingly, due to the growth of the maize plants, the footprint of the spectral measurements decreased slightly from a circle with ~5.1 m diameter to a circle with ~ 4.4 m diameter. Because the canopy conditions were homogeneous, we assumed that these slight changes in footprint would not have much influence on SIF retrievals.

2.5.2. Remote sensing of vegetation indices

All VIs calculated from the reflectance collected by the FluoSpec2 system were used to track structure, pigments, and physiological changes in the maize canopy. The red edge normalized difference vegetation index (Rededge NDVI) is an index that correlates well with $fPAR_{chl}$ (Viña and Gitelson, 2005). The scaled Rededge NDVI was used as a proxy of $fPAR_{chl}$ (Eq. (3)). The modified triangular vegetation index (MTVI2), which can minimize the effect of variations in leaf chlorophyll content (Haboudane et al., 2004), was used to track changes in green LAI of maize canopy. The equations of the VIs are listed in Table 1.

$APAR_{chl}$ is the photosynthetic active radiation absorbed by chlorophyll and was calculated according to equation (3) (Zhang et al., 2018b; Miao et al., 2018):

$$\begin{cases} fPAR_{chl} = 1.37 \times Rededge\ NDVI - 0.17 \\ APAR_{chl} = PAR \times fPAR_{chl} \end{cases} \tag{3}$$

where $fPAR_{chl}$ represents the fraction of PAR absorbed by chlorophyll of the maize canopy. The SIF_{yield} and LUE were derived as $SIF/APAR_{chl}$ and $GPP/APAR_{chl}$, respectively.

2.5.3. Analysis of environmental conditions

Sunny days and cloudy days were differentiated using the clearness index (CI) (Kumar & Umanand, 2005), which was calculated as the ratio of the global solar radiation on the surface of the planet (R_g) to the extraterrestrial radiation at the top of the atmosphere (R_0). R_0 at the maize field was calculated using the solar zenith angle (θ) as:

$$R_0 = S_0 \times (1 + \cos(360 \times DOY/365))/\cos\theta \tag{4}$$

where S_0 is the solar constant (1367 W/m^2). R_g is the solar shortwave radiation measured using a net radiometer (CNR1, Kipp & Zonen, Netherlands). A commonly used threshold of 0.5 was applied to distinguish sunny (daily mean CI $>$ 0.5) and cloudy days (daily mean CI $\leq$ 0.5). In addition, half-hourly mean CI $>$ 0.5 indicated a clear sky within the half hour, whereas half-hourly mean CI $\leq$ 0.5 represented a cloudy sky within the half hour.

2.5.4. Decomposing the canopy structure effects on SIF_{yield}

Leaf area index (LAI) proposed by Chen and Black (1992) is defined as half the total area of green elements of the canopy per unit horizontal ground area. This definition effectively describes the canopy structure and is robust for different vegetation shapes (Weiss et al., 2003). We measured *in situ* LAI on DOY 201, 215, 227, 237, 248, and 262 with a LAI-2000 plant canopy analyzer (LI-COR, Inc., Lincoln, NE, USA) at nightfall. According to the measurements, MTVI2 explained 83% of the variations in LAI of the maize canopy (Fig. S1), indicating that MTVI2

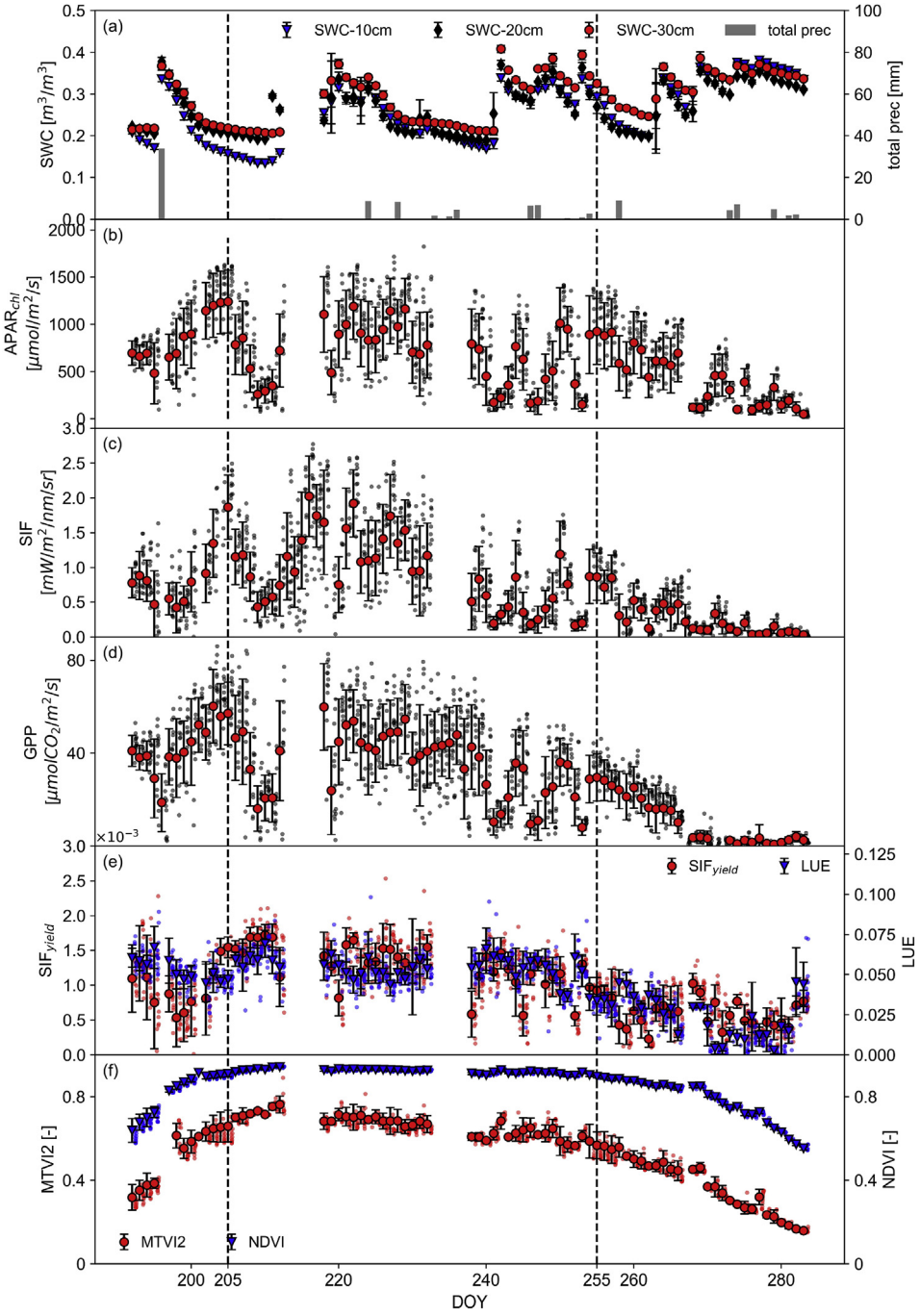

Fig. 2. Seasonal patterns of (a) soil water content (SWC) at three soil depths (10 cm, 20 cm and 30 cm) and total precipitation (gray bars), (b) PAR absorbed by chlorophyll ($APAR_{chl}$), (c) solar-induced fluorescence (SIF), (d) gross primary productivity (GPP), (e) solar-induced fluorescence yield (SIF_{yield}) and light use efficiency (LUE), (f) the modified triangular vegetation index (MTVI2) and normalized difference vegetation index (NDVI) derived from FluoSpec2 system measurements. Small dots represent half-hourly mean values; big markers and error bars indicate daily means and standard deviations, respectively. Daily means and standard deviations were calculated from all half-hourly values in the day. Two dashed black lines indicate the beginning of the reproductive and ripening growth stages, respectively.

could describe most of the variations in maize canopy LAI. Since we only had *in-situ* LAI data measured on six separate days over the season, we used MTVI2 to represent the seasonal LAI of the canopy.

To study the effects of canopy structure on SIF_{yield} and LUE, we defined LAI-scaled SIF_{yield} (hereafter, $rSIF_{yield}$) to eliminate the influences of canopy structure, where MTVI2 is used as a proxy of LAI (Haboudane et al., 2004). The $rSIF_{yield}$ was calculated as:

Table 1
Vegetation indices (VIs) used in this study. r_{NIR}, r_{red} and $r_{rededge}$ refer to reflectance derived from spectral data collected by Path 2 of the FluoSpec2 system in bands of 770–790 nm, 650–680 nm, 700–710 nm, respectively. The r_λ is the reflectance at the given wavelength λ.

Vegetation index	Formula	Reference
Normalized difference vegetation index (NDVI)	$\frac{r_{NIR}-r_{red}}{r_{NIR}+r_{red}}$	Rouse et al., (1973)
Red edge Normalized different vegetation index (Rededge NDVI)	$\frac{r_{NIR}-r_{rededge}}{r_{NIR}+r_{rededge}}$	Viña and Gitelson, (2005)
Modified triangular vegetation index (MTVI2)	$1.5\times\frac{1.2\times(r_{800}-r_{550})-2.5\times(r_{670}-r_{550})}{\sqrt{(2\times r_{800}+1)2-(6\times r_{800}-5\times\sqrt{r_{670}})-0.5}}$	Haboudane et al., (2004)

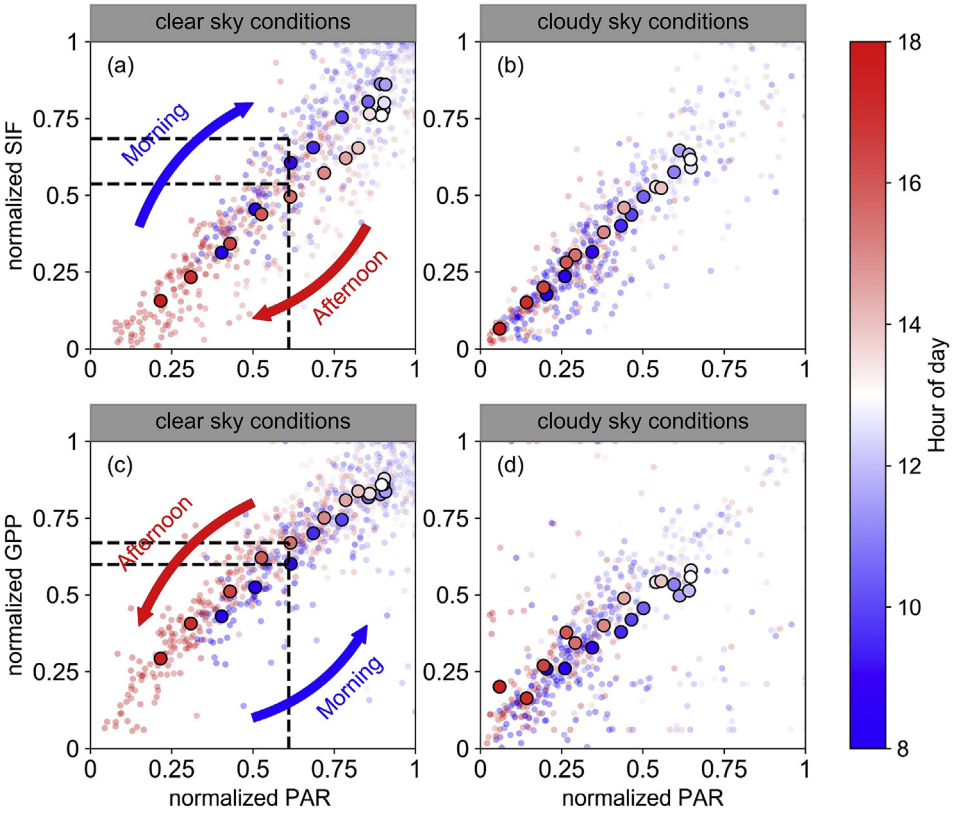

Fig. 3. Average diurnal patterns of normalized SIF (half-hour SIF/maximum SIF for each day) and normalized GPP (half-hour GPP/maximum GPP for each day) in response to normalized PAR (half-hour PAR/maximum PAR for each day) in clear sky conditions and cloudy sky conditions during the growing season of maize. SIF and PAR under sunny (a) and cloudy days (b). GPP and PAR under sunny (c) and cloudy days (d). The large dots represent the average diurnal pattern of the small light-colored dots. The color bar represents the hour of the day. (For interpretation of the references to color in this figure legend, the reader is referred to the Web version of this article.)

$$rSIF_{yield} = SIF_{yield}/\text{normalized MTVI2} \quad (5)$$

where normalized MTVI2 was calculated as:

$$\text{normalized MTVI2} = \frac{\text{MTVI2} - \text{MTVI2}_{min}}{\text{MTVI2}_{max} - \text{MTVI2}_{min}} \quad (6)$$

where $MTVI2_{min}$ and $MTVI2_{max}$ were the minimum and maximum of the MTVI2 during the growing season.

2.5.5. Statistical analysis

Apart from the quality control (c.f. Section 2.2) of the raw measured spectral data of SIF retrievals, additional outliers were removed using a moving window with 30 min width. Within the 30 min window, values above (μ + 3σ) or below (μ-3σ) were excluded, where μ and σ are the average and standard deviation, respectively. Then, the half-hourly mean was calculated as the average of the data within the 30 min window. The daily mean value was calculated as the average of all half-hourly mean values in the day.

In addition, it has to be noted that despite the quality control and extra outliers exclusion conducted before and after the SIF retrieval, there may be still uncertainties in SIF retrievals. The uncertainty of the retrieved SIF was defined as the relative standard deviation within a 30 min window. The minimum, maximum, average, and standard deviation of the uncertainty in a typical sunny day were 1.59%, 5.05%, 2.95%, and 1.15%, respectively. In a typical cloudy day, the minimum, maximum, average, and standard deviation of the uncertainty were 8.72%, 56.86%, 17.76%, and 11.93%, respectively.

The EC flux data were processed every 30 min of 24 h from June 6th to October 10th, 2017. Simultaneous SIF data were chosen from every 30 min from July 11th to November 15th, 2017. Overall, 82 days of data (including 45 sunny days and 37 cloudy days) were available in this study within the 92 days study period (July 11th to October 10th). Days (10 days in all) when EC flux data or spectral data were incomplete or rainfall occurred were excluded. Statistical analysis and visualization of this study were performed using Matlab R2016b (MathWorks, USA) and Python 3.6.1 (Python Software Foundation, USA).

3. Results

3.1. Seasonal and diurnal variations of SIF, GPP, and VIs at the canopy level

The maize plants did not suffer from water stress during the growing season in 2017 thanks to precipitation received and supplemental irrigation (Fig. 2a). The maize canopy showed conspicuous seasonal variations in $APAR_{chl}$, SIF, and GPP (Fig. 2b–d), which were mostly due to the seasonal evolutions of incoming radiations and plant growth stages. Fluctuations in SIF and GPP were primarily driven by the variations of $APAR_{chl}$, which explained 77% and 81% of the variances in SIF and GPP, respectively (Fig. S2). Both SIF and GPP gradually increased from 1 mW/m^2/nm/sr and 40 μmol CO_2/m^2/s at the beginning of the growing season to 2.5 mW/m^2/nm/sr and 60 μmol CO_2/m^2/s until around DOY 205, when the maize canopy almost reached its maximal development. During the reproductive stage, SIF and GPP maintained their maximum values for several days when $APAR_{chl}$ was high and stable, but also decreased considerably during cloudy conditions. During the ripening stage, both SIF and GPP declined to 0 due to decreasing $APAR_{chl}$ and leaf senescence.

Fig. 2e shows the seasonal pattern of SIF_{yield} and LUE. Both SIF_{yield} and LUE decreased in the vegetative stage, remained relatively stable in the reproductive stage and in the early ripening stage and increased in the late ripening stage (Fig. 2e). The seasonal patterns of MTVI2 and NDVI show that these VIs increased in the vegetative stage, remained relatively stable in the reproductive stage and decreased in the late ripening stage (Fig. 2f). Compared to SIF and GPP, seasonal fluctuations of VIs were relatively small especially during the reproductive stage, in which SIF and GPP mostly vary with PAR (i.e. weather conditions) while VIs, SIF_{yield} and LUE remained relatively stable. Diurnal variations of SIF, GPP, NDVI, and PAR for the maize canopy are shown in Fig. S3 for some clear and cloudy days during the growing season. SIF

showed a strong diurnal pattern, which was mainly driven by the incoming radiation with maximum values around midday. On the other hand, the diurnal NDVI showed a slight diurnal pattern, which was less variable than that of SIF on both sunny and cloudy days (Fig. S3d).

We also explored the diurnal patterns of SIF in response to incoming irradiance. We used normalized values to eliminate the influence of seasonal variations in absorbed PAR (Fig. 3). During clear-sky conditions, a diurnal hysteresis was observed between SIF and PAR for maize over the course of the characterized day (Fig. 3a). This hysteresis showed a clockwise looping pattern between SIF and PAR, which indicated a higher canopy SIF in the morning than in the afternoon at similar incident solar radiance values. On the contrary, this hysteretic phenomenon was not observed on cloudy days (Fig. 3b). In contrast to the diurnal clockwise looping pattern of SIF-PAR, a slight counterclockwise looping pattern was observed for GPP and PAR during sunny days, though this pattern was less obvious (Fig. 3c). This asymmetry of GPP-PAR was not observed on cloudy days (Fig. 3d).

The asymmetry and asynchronism of the diurnal variation of SIF in response to PAR shown in Fig. 3a may result in some uncertainties for using a daily correction method to estimate daily mean SIF (Frankenberg et al., 2011; Sun et al., 2018). Considering that satellite SIF are generally observed under clear-sky conditions, we chose all half-hourly data under clear sky conditions and calculated the average diurnal apparent SIF_{yield} (SIF/PAR) during the three growth stages and the whole season (Fig. 4). More obviously, the diurnal hysteresis was observed, with higher apparent SIF_{yield} in the morning than in the afternoon in all three growth stages and over the whole season. We chose the instantaneous fitted apparent SIF_{yield} at 13:30 h (red dots in Fig. 4a–d, which is approximately the overpass time of OCO-2 satellite) to upscale instantaneous SIF (SIF_{inst}) to daily mean SIF (SIF_{daily}) (Fig. 4e–h). The gray shaded region between the retrieved SIF and daily corrected SIF represented the bias. SIF_{daily} was underestimated over the three growth stages, and hence for the whole season (underestimations were 6.65%, 2.37%, 12.67%, and 4.74%, respectively). Moreover, larger underestimations were observed in the morning (the gray rectangle area, underestimations were 12.77%, 7.01%, 26.48%, and 12.07%, respectively) due to higher apparent SIF_{yield} in the morning than in the afternoon (e.g., 13:30).

3.2. Effects of crop growth stages on the GPP-SIF relationship

Strong correlations between SIF and GPP over the season at multiple temporal resolutions were observed for the maize canopy (Fig. 5). For half-hourly data, an convex shape curve fitting of SIF and GPP could be clearly visible for both cloudy and sunny days, which indicates a non-linear relationship between SIF and GPP at half-hourly temporal resolution. The relationship between SIF and GPP showed an improvement when aggregating half-hourly to daily and 8-day (R^2 increased from 0.67 to 0.80 and 0.90, Fig. 5a). Over the whole growing season, the slope of the SIF-GPP relationship at 8-day timescale was significantly larger than that of one day for all days (Fig. 5a, daily (1d): k = 31.89, 8-day (8d): k = 36.62, 14.83% higher), clear sky days (Figs. 5b, 1d: k = 23.98, 8d: k = 26.37, 9.97% higher), and for cloudy days (Figs. 5c, 1d: k = 43.03, 8d: k = 46.29, 7.58% higher). In addition, radiation also had an influence on the slope of the regression of SIF and GPP. The regression slope for cloudy days was much larger than that for clear sky days under two temporal resolutions (1d: k = 43.03 for cloudy days and k = 23.98 for clear days, Fig. 5b and c; 8d: k = 46.29 for cloudy days and k = 26.37 for clear days, Fig. 5b and c) and different growth stages (Fig. 6).

To determine how crop growth stage impacted the relationship of SIF to GPP, we examined the differences of the GPP-SIF relationship across the three growth stages. SIF showed a positive correlation with GPP at both half-hourly and daily time scales, but the slope of the linear regression between GPP and SIF varied significantly among different crop growth stages (Fig. 6). We observe that the slopes of the linear regressions of SIF and GPP for the three growth stages increased throughout the growing season (Fig. 6d–f). Additionally, during the ripening stage, both SIF and GPP showed much lower values on sunny days even though the incoming radiation was still high (Fig. S3). This indicates a decrease in SIF_{yield} and LUE due to leaf senescence, which is consistent with Fig. 4e.

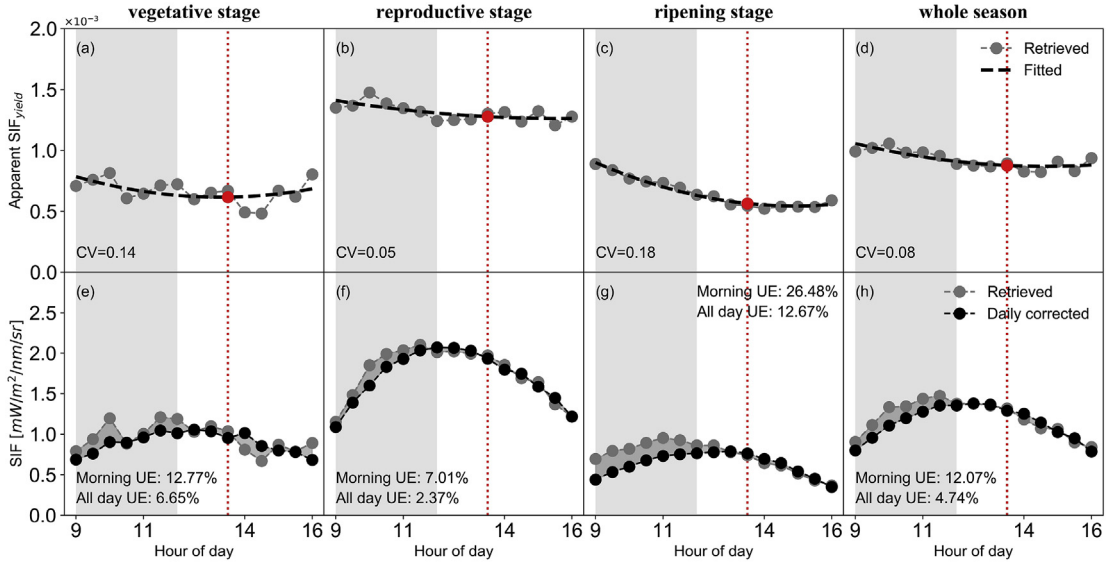

Fig. 4. Diurnal patterns of apparent SIF_{yield} (i.e. SIF/PAR) under clear-sky conditions during three growth stages and whole season (a–d). Corresponding diurnal patterns of retrieved SIF (gray line) and daily corrected SIF (black line) using retrieved SIF_{yield} at 13:30 (i.e. the overpass time of OCO-2) in three growth stages and whole season (e–h). The gray shaded region between the two lines in (e–h) is the difference between retrieved SIF and corrected SIF. The dashed gray line is the quadratic fitted line of diurnal apparent SIF_{yield}. The vertical dashed red line represents the time of 13:30. The red dot is the point of intersection of the vertical dashed line and fitted line, representing the fitted apparent SIF_{yield} value at 13:30 which was used for upscaling in this study. CV is the coefficient of variance. All day UE and Morning UE represent the amount of underestimations for the whole day and in the morning, respectively. (For interpretation of the references to color in this figure legend, the reader is referred to the Web version of this article.)

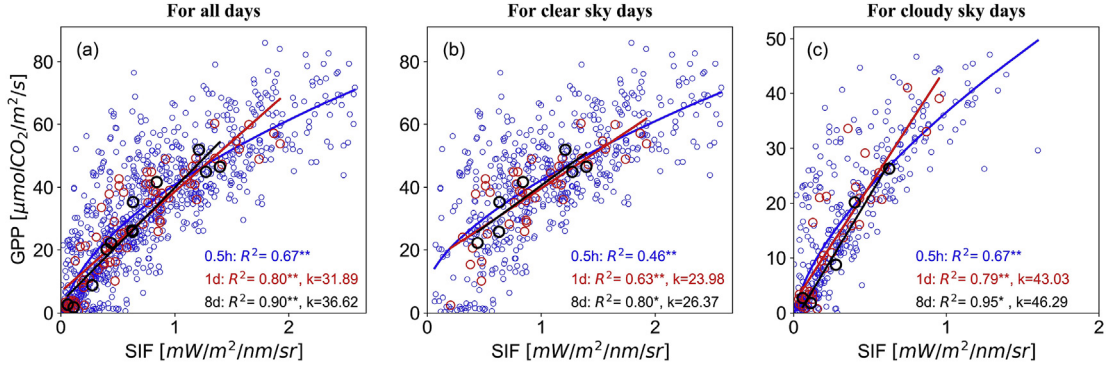

Fig. 5. Relationships between SIF and GPP at half-hourly (blue circles), daily (red circles) and 8-day timescale (black circles) (a) for all days, (b) for clear sky days, (c) for cloudy sky days. The red line and black line are linear regressions for daily data (1d) and 8-day steps data (8d), respectively. The blue curve is a power model fit for the hourly data (1h). R^2 and k represent the coefficient of determination and slope of the linear regression, respectively. All R^2 values were statistically significant (* for $p < 0.05$, ** for $p < 0.001$). (For interpretation of the references to color in this figure legend, the reader is referred to the Web version of this article.)

3.3. *Effects of crop growth stages on the LUE-SIF_{yield} relationship*

Considering the joint influence of environmental conditions and growth stages on the SIF-GPP relationship, we analyzed the effects of growth stage on the LUE-SIF_{yield} relationship by alleviating the effects of incident radiation (Fig. 7). LUE and SIF_{yield} showed a significant dispersion during the three growth stages with minor variability of MTVI2 (LAI proxy) in each stage (Fig. 7a–c; $R^2 < 0.1$). However, a significantly positive LUE-SIF_{yiled} correlation was observed in Fig. 7d ($R^2 = 0.26$) at the half-hourly time scale over the whole growing season. LUE increased linearly with SIF_{yield} as MTVI2 also increased. The correlation between LUE and SIF_{yield} for the whole season was even stronger at the daily time scale ($R^2 = 0.46$; Fig. 7h).

For a better understanding of the effects of canopy structure on the LUE_SIF_{yield} relationship, we present the relationships between LUE and $rSIF_{yield}$ (c.f. Section 2.5.4) at half-hourly and daily scales in Fig. 8. By scaling SIF_{yield} with the normalized MTVI2, the influence of the changing LAI on SIF_{yield} was largely alleviated due to the significantly low relationship between $rSIF_{yield}$ and MTVI2 (Fig. S4). Clear differences in the relationship between $rSIF_{yield}$ and LUE compared with that between SIF_{yield} and LUE were observed (Fig. 8). After controlling for the effects of changing LAI, $rSIF_{yield}$ and LUE became almost unrelated at both half-hourly and daily time scale (Fig. 8). Overall, our findings highlight the strong canopy structure related influences of phenological stages on the seasonal changes of SIF_{yield} and LUE as well as their link. This strong influence is similar for both sunny and cloudy days (Fig. S5, S6).

4. Discussion

A number of recent studies have demonstrated that SIF and GPP

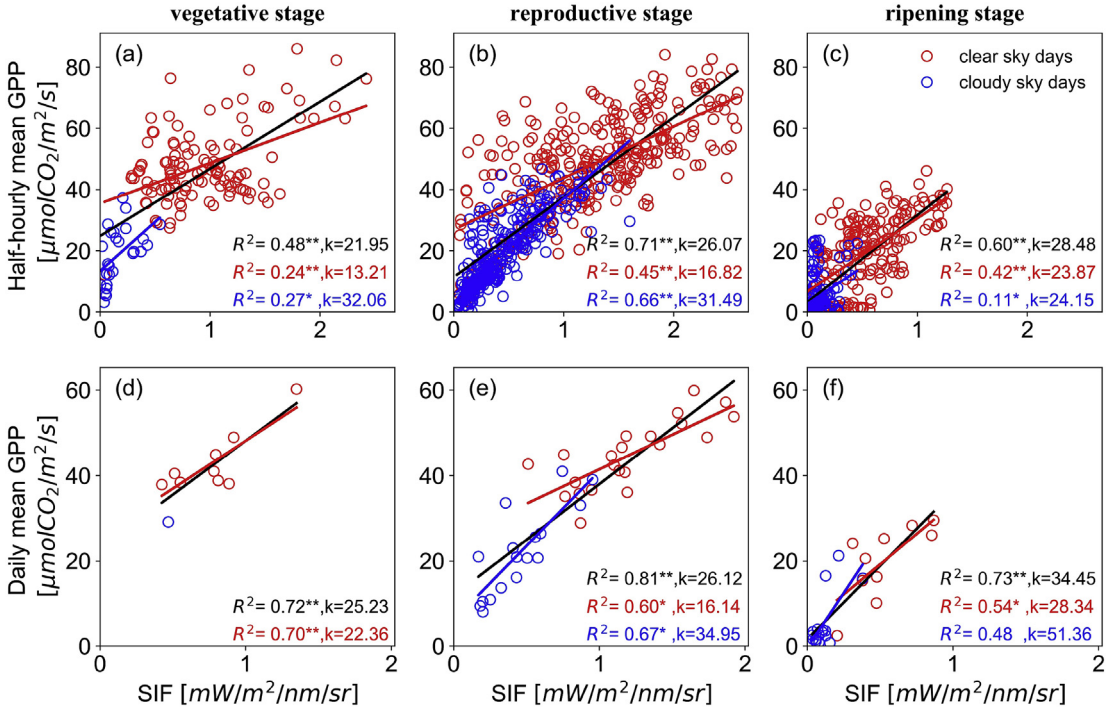

Fig. 6. Relationships between SIF and GPP based on the 30 min data (a–c) and daily mean data (d–f) during the three growth stages. Red circles represent clear sky days, and blue circles represents cloudy sky days. The red line and blue line are linear regressions for clear sky data and cloudy sky data, respectively. The black line is the linear regression for all data in the stage. R^2 and k represent the coefficient of determination and slope of the linear regression, respectively. All R^2 values were statistically significant (* for $p < 0.05$, ** for $p < 0.001$). (For interpretation of the references to color in this figure legend, the reader is referred to the Web version of this article.)

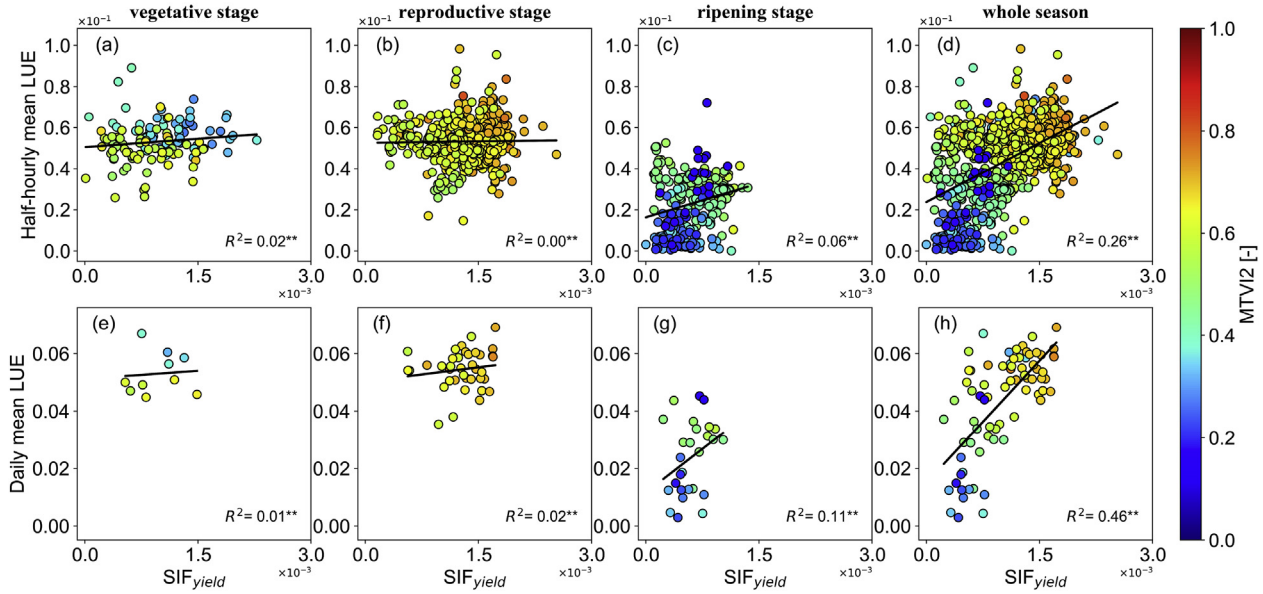

Fig. 7. Relationships between SIF_{yield} and LUE based on 30 min data (a–d) and daily mean data (e–h) during the three growth stages and whole season. Linear regression lines are shown in black. The color bar represents MTVI2. R^2 represents the coefficient of determination. All R^2 values were statistically significant (* for $p < 0.05$, ** for $p < 0.001$). (For interpretation of the references to color in this figure legend, the reader is referred to the Web version of this article.)

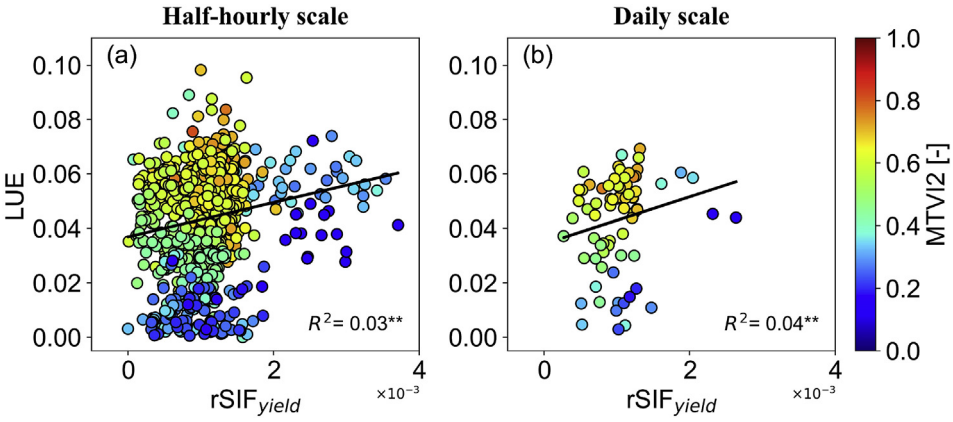

Fig. 8. Relationships between $rSIF_{yield}$ and LUE at (a) half-hourly and (b) daily scale across the growing season. Linear regression lines are shown in black. The color bar represents MTVI2. R^2 represents the coefficient of determination. All R^2 values were statistically significant (** for $p < 0.001$). (For interpretation of the references to color in this figure legend, the reader is referred to the Web version of this article.)

share a strong positive relationship at multiple spatial scales (e.g., Frankenberg et al., 2011; Guanter et al., 2014; Yang et al., 2015; Sun et al., 2018). Taking advantage of the recent advances in automatic ground-based spectroscopy measurements (e.g., Yang et al., 2018a), we collected continuous and long-term canopy SIF at high temporal resolution during a growing season of maize in 2017, which were used to investigate the seasonal variations of SIF and their relation to GPP for different growth stages.

4.1. Comparison on the relationships of SIF & GPP, SIF_{yield} & LUE with other ecosystems

Overall, our results are consistent with previous results for both C3 (Verma et al., 2017; Damm et al., 2010, 2015; Yang et al., 2015; Zarco-Tejada et al., 2013) and C4 ecosystems (Wagle et al., 2016). During the growing season, the significantly strong correlations between SIF and GPP denote that SIF is well correlated to GPP at multiple temporal scales. However, the relationships of SIF and GPP change from non-linear to linear as the temporal resolution changes from half-hourly to daily or 8-days. This transition may be related to several factors that influence the SIF-GPP relationship, such as the physiological status, vegetation biochemistry (e.g. leaf pigments, water and dry matter), canopy structure (Du et al., 2017; Van der Tol et al., 2014; Yang and Van der Tol., 2018), environmental conditions (Verma et al., 2017; Miao et al., 2018), and observation angles (Liu et al., 2016). The impact of these factors is reduced to some extent when integrating data from high temporal resolution to low temporal resolution. The nonlinear relation between SIF and GPP could also be explained by structural effects. At the half-hourly scale, SIF scattering and re-absorption of the canopy are considerable.

We also found that the slope of the SIF-GPP relationship for C4 plants is higher than that for C3 plants (Yang et al., 2018a), which is consistent with findings based on both field and space-borne measurements at multiple time scales (Wood et al., 2017; Liu et al., 2017; Zhang et al., 2016). The slope difference between C3 and C4 plants is an indicator of the difference between LUE and SIF_{yield}. Liu et al. (2017) investigated the diurnal cycles of flux tower GPP estimates and SIF observations at 760 nm for wheat (C3) and maize (C4) canopies. They found that LUE for C4 maize is much higher than that for C3 wheat while SIF_{yield} is relatively similar. This indicates that similar SIF_{yield} but large difference in LUE between C3 and C4 crops lead to the difference in the slopes of the SIF-GPP relationship at the canopy scale. In addition, we found that the slope of the SIF-GPP relationship is larger under cloudy sky conditions, which is consistent with findings in rice paddy (Yang et al., 2018a) and in a winter-dormant evergreen conifer forest (Magney et al., 2019). This could be largely explained by more efficient

use of diffuse radiation by plants, which results in higher GPP under cloudy or aerosol-laden skies (Gu et al., 1999, 2002; Still et al., 2009) while SIF_{yield} remains relatively constant (Frankenberg, C., & Berry, J.K., 2018). Besides, larger uncertainties of retrieved SIF in cloudy conditions are not negligible. The slope may increase if the SIF is underestimated under diffuse light conditions.

At the seasonal scale, we found a positive correlation between daily mean SIF_{yield} and LUE for maize, with R^2 close to 0.46 (Fig. 7h). This is generally in agreement with several recent studies for deciduous forest (Yang et al., 2015), wheat (Goulas et al., 2017), rice (Yang et al., 2018a) based on ground measurements, and a C4 grassland (Verma et al., 2017) based on satellite measurements. However, we found a slightly higher correlation between SIF-GPP than SIF- $APAR_{chl}$ for daily mean values (R^2 = 0.80 and 0.77, respectively, Fig. 5a, Fig. S3). This is inconsistent with findings supported by several studies based on C3 crop measurements (Yang et al., 2015, 2018a; Miao et al., 2018; Wieneke et al., 2018). This indicates a stronger SIF_{yield}-LUE relationship for C4 crops than for C3 crops (Fig. 7h).

4.2. Influence of crop growth stages on the SIF-GPP relationship

In this study, we found that the SIF-GPP relationship changed (as evidenced by changes in R^2 and slope of the linear regression) depending on the growth stage. These changes may be attributed to the joint influences of environmental conditions and phenological stages. SIF retrievedd at TOC is a product of a series of processes, including (1) absorption of PAR by canopy chlorophyll (Zhang et al., 2018), (2) SIF emission accompanying photosynthesis (Van der Tol et al., 2014), and (3) scattering and re-absorption of SIF in the canopy (Yang and van der Tol, 2018; Yang et al., 2018b). We argue that environmental conditions mainly affect the first two processes through changing incoming radiation, which is the first order driving factor that influences both SIF and GPP. As a result, the SIF-GPP relationship changes depending on the environmental conditions (different R^2 and slope in sunny and cloudy days; Figs. 5, 6). In addition, the phenological stage (characterized by canopy structure) mainly influences the third process. SIF scattering and re-absorption are sensitive to canopy structure, including canopy LAI and leaf orientation (Verrelst et al., 2015, 2016). This could be mainly related to canopy structure effects influencing the fraction of SIF escaping the canopy (f_{esc}). Therefore, canopy structure is crucial when linking SIF and photosynthesis for GPP estimations (Yang and van der Tol, 2018).

In this study, LAI of maize showed an obvious seasonal variation (Fig. 2). Variations of LAI and physiological status of maize are expected to influence the seasonal variation of f_{esc}, which in turn affects the SIF-GPP relationship. Therefore, quantifying the f_{esc} of canopy SIF accurately can improve the mechanistic understanding of the link between SIF and GPP. However, determining the precise contribution of each factor to the changes in the SIF-GPP relationship is challenging. Yang and van der Tol (2018) provided an approach to mitigate the effect of canopy structure as well as bidirectional effects, which may lead to a future deeper understanding of the canopy SIF-GPP relationship. They found that the canopy structural effects on SIF can be precisely estimated by $\frac{R_{far-red}}{i_0 \times \omega}$, where $R_{far-red}$, i_0, and ω represent the reflectance in the far-red band, canopy interception and leaf albedo, respectively. Similarly, Zeng et al. (2019) estimated the effects of canopy structure based on near-infrared reflectance of vegetation and fPAR. These approaches may provide promising prospects for a greater understanding of the underlying process for the SIF-GPP and SIF_{yield}-LUE relationships in future studies.

4.3. Influence of canopy structure on the LUE-SIF_{yield} relationship

We analyzed the effects of the growth stages on the LUE-SIF_{yield} relationship by partitioning a whole growing season of maize into three individual growth stages. Obviously, changes in the growth stages led to changes of the canopy structure, explaining most of the strong correlation between seasonal LUE and SIF_{yield} (Fig. 7). We showed that seasonal variations of SIF_{yield} and LUE respond similarly to the canopy structure, and generally increase with MTVI2. This result is supported by several recent simulation and observation-based studies. Wieneke et al. (2018) also found that SIF_{yield} is affected by seasonal changes of canopy structure for sugar beets based on measurements.

In addition, we compensated for the effects of crop growth stage on the LUE-SIF_{yield} relationship by using MTVI2. In this way, the large difference in the correlation between LUE-SIF_{yield} and LUE-rSIF_{yield} results exclusively from the influence of canopy structure on SIF_{yield}. This result points to the significant role of canopy structure in linking LUE and SIF_{yield}. Our finding here is consistent with the recent work by Wieneke et al. (2018), which also found a significant reduction in the relationship between SIF_{yield} and LUE after compensating for the influence of changing canopy structure. However, they found that there is still a slight correlation between diurnal LUE and SIF_{yield} (R^2 = 0.1, $P < 0.05$) under non-stressed conditions with the correction of canopy structure effects.

Recently, several studies have reported the influence of canopy structure on the SIF signals at the TOC (Liu et al., 2018b; Yang and van der Tol, 2018). The radiative transfer process of SIF at TOC can be expressed with Eq. (7):

$$SIF = APAR_{chl} \times \varnothing_F \times f_{esc} \quad (7)$$

where $\varnothing_F$ represents the quantum yield of fluorescence. The SIF_{yield} we calculated is, in fact, the product of the $\varnothing_F$ times the escape probability f_{esc}. The escaping process of SIF is determined by the scattering and re-absorption of SIF within the canopy, which are sensitive to the canopy structure, including canopy LAI and leaf orientation (Verrelst et al., 2015, 2016). Consequently, the derived SIF_{yield} and LUE-SIF_{yield} relationship can be largely influenced by the changes of canopy structure with changing LAI and leaf orientation. Therefore, it is essential to decouple the effects of canopy structure before physiological changes can be interpreted using canopy SIF across multiple temporal scales (Yang et al., 2018b).

Our results suggest the potential of concurrent hyper-spectral (400–1000 nm) measurements and SIF signals retrieval for studying ecosystem functioning and canopy photosynthesis. The combination of reflectance and SIF enables us to advance the analysis of canopy structure, SIF observations, and their link to photosynthesis (Miao et al., 2018; Yang et al., 2018b; Zeng et al., 2019). We can calculate MTVI2 as a proxy of LAI using hyperspectral data to compensate the effects of canopy structure on canopy SIF and to advance the analysis of canopy SIF observations. A more explicit relationship between SIF and GPP would help understand the link between fluorescence, photosynthesis, and NPQ both at canopy and at leaf level.

4.4. Implications for temporal scaling of SIF from satellite measurements

We found a diurnal hysteresis in apparent SIF_{yield}, with higher apparent SIF_{yield} in the morning than in the afternoon under similar insolation conditions in a maize field (Figs. 3, 4). A similar finding was also recently observed in a deciduous broadleaf forest (C3) (Gu et al., 2018) and crop field (C3) (Wieneke et al., 2018). The diurnal variation of apparent SIF_{yield} is complex. Solar energy absorbed by pigments of PSII is consumed through three main pathways: photosynthesis, NPQ, and fluorescence (Porcar-Castell et al., 2014). Excess light affects electron transport rate which then affects the carbon fixation in the calvin cycle in photosynthesis. During a sunny day, carbon fixation reactions and electron transport chain reach a light saturation when the light level increases, which limits photosynthesis (Porcar-Castell et al., 2014). The quantum yield of fluorescence may decrease due to the increasing NPQ. When the light level decreases, SIF_{yield} increases slightly as photosynthesis and NPQ decrease. We also speculate that

NPQ in the afternoon is relatively higher than in the morning. Therefore, SIF_{yield} seems to be higher in the morning than in the afternoon if we assume photosynthesis to be constant under the same light level (Porcar-Castell et al., 2014). In addition, the difference in sunlit fraction that the sensor detects can also be a potential factor for the observed asymmetry. Although the SIF signals were collected at nadir, there may be still a difference in the fraction of sunlit leaves in the morning and afternoon owing to the influences of leaf inclination angle and solar zenith angle.

This hysteresis of apparent SIF_{yield} may lead to uncertainties of the upscaling of satellite retrieved SIF. Currently, there are several methods for upscaling SIF_{inst} to SIF_{daily}, such as $SIF_{inst} \times \frac{PAR_{daily}}{PAR_{inst}}$ and $SIF_{inst} \times \frac{\cos(SZA)_{daily}}{\cos(SZA)_{inst}}$ (Sun et al., 2018; Hu et al., 2018; Zhang et al., 2018a). However, both methods assume that the SIF_{yield} and fPAR have much smaller diurnal variations compared to PAR. Our results suggest that there are potential errors in these upscaling methods. Our findings also indicated that SIF_{daily} was mostly underestimated due to the asymmetric pattern of diurnal SIF_{yield} to PAR (Figs. 3, 4). Furthermore, this underestimation of SIF_{daily} is related to the time periods (large underestimations in the morning) and phenology (Fig. 4). This means that SIF_{daily} derived from instantaneous SIF based on satellite data acquired at different phenological stages may be underestimated to varying degrees. Zhang et al. (2018a) found that the conversion factor (i.e. $\frac{PAR_{daily}}{PAR_{inst}}$ or $\frac{\cos(SZA)_{daily}}{\cos(SZA)_{inst}}$) between SIF_{inst} and SIF_{daily} is related to latitude, which means that the underestimation of SIF_{daily} can also change with latitude. Therefore, the spatial and seasonal relationship between GPP and temporally upscaled satellite SIF may be more complicated.

5. Conclusion

In this study, we investigated canopy structural effects on SIF-GPP and SIF_{yield}-LUE relationships based on continuous measurements in a maize field in 2017. A strong linear relationship between SIF and GPP was found for maize at daily and 8-days temporal resolution over the growing season, while the relationship was curvilinear at half-hourly temporal resolution for both sunny and cloudy days. At the sub-seasonal scale, the relationship between SIF and GPP varied with different crop growth stages for maize at multiple temporal resolutions, which suggests that canopy structure plays an import role in the seasonal variations of canopy SIF and their relation to GPP. Importantly, our results showed that the observed significant relationship between canopy SIF_{yield} and LUE across the season was dominated by seasonal variations in canopy structure in maize. After compensating for the effects of canopy structure with the structural vegetation index MTVI2, SIF_{yield} and LUE tended to become uncorrelated at the seasonal scale. In addition, we found that there was a typical diurnal hysteresis in apparent SIF_{yield} in response to PAR across the whole growing season, with higher apparent SIF_{yield} in the morning than in the afternoon under the same incoming radiance. These results highlight the importance of quantifying bias in upscaling instantaneous SIF from a snapshot once in a day to daily mean. Our observation-based findings can help strengthen our understanding on the mechanistic link between canopy SIF and photosynthesis. However, additional measurements for different vegetation types are necessary for fully understanding the effects of canopy structure on SIF signals in other terrestrial ecosystems.

Acknowledgments

This research was financially supported by National Natural Science Foundation of China (41671421 and 41701393), International Cooperation and Exchange Programs between NSFC and DFG (41761134082), Jiangsu Provincial Natural Science Fund for Distinguished Young Scholars of China (BK20170018), and Natural Science Foundation of Jiangsu Province for Youth (BK20170641). We would thank Ms. Jing Li, Mr. Shihua Zhu from Nanjing University and Mr. Pengju Wu and other researchers from ShangQiu station of Farmland Irrigation Research Institute of Chinese Academy of Agricultural Sciences for the field measurements. We also would thank Dr. Cristina Milesi for the professional and elaborate proof-reading work for this manuscript.

Appendix A. Supplementary data

Supplementary data to this article can be found online at https://doi.org/10.1016/j.rse.2019.111420.

References

Alcaraz, M.L., Thorp, T.G., Hormaza, J.I., 2013. Phenological growth stages of avocado (persea americana) according to the bbch scale. Sci. Hortic. 164, 434–439.
Baldocchi, D.D., Hincks, B.B., Meyers, T.P., 1988. Measuring biosphere-atmosphere exchanges of biologically related gases with micrometeorological methods. Ecology 69, 1331–1340.
Baldocchi, D.D., Vogel, C.A., Hall, B., 1997. Seasonal variation of carbon dioxide exchange rates above and below a boreal jack pine forest. Agric. For. Meteorol. 83, 147–170.
Chen, J.M., Black, T.A., 1992. Defining leaf area index for non-flat leaves. Plant Cell Environ. 15, 421–429.
Chen, B., Black, T.A., Coops, N.C., Hilker, T., Trofymow, J.A., Morgenstern, K., 2009. Assessing tower flux footprint climatology and scaling between remotely sensed and eddy covariance measurements. Boundary-Layer Meteorol. 130 (2), 137–167.
Cogliati, S., Verhoef, W., Kraft, S., Sabater, N., Alonso, L., Vicent, J., Moreno, J., Drusch, M., Colombo, R., 2015. Retrieval of sun-induced fluorescence using advanced spectral fitting methods. Remote Sens. Environ. 169, 344–357.
Damm, A., Elbers, J., ANDRé, E.R.L.E.R., Gioli, B., Hamdi, K., Hutjes, R., et al., 2010. Remote sensing of sun-induced fluorescence to improve modeling of diurnal courses of gross primary production (gpp). Glob. Chang. Biol. 16 (1), 171–186.
Damm, A., Guanter, L., Laurent, V.C.E., Schaepman, M.E., Schickling, A., Rascher, U., 2014. FLD-based retrieval of sun-induced chlorophyll fluorescence from medium spectral resolution airborne spectroscopy data. Remote Sens. Environ. 147, 256–266.
Damm, A., Guanter, L., Paul-Limoges, E., van der Tol, C., Hueni, A., Buchmann, N., Eugster, W., Ammann, C., Schaepman, M.E., 2015. Far-red sun-induced chlorophyll fluorescence shows ecosystem-specific relationships to gross primary production: an assessment based on observational and modeling approaches. Remote Sens. Environ. 166, 91–105.
Daumard, F., Champagne, S., Fournier, A., Goulas, Y., Ounis, A., Hanocq, J., Moya, I., 2010. A field platform for continuous measurement of canopy fluorescence. IEEE Trans. Geosci. Remote Sens. 48, 3358–3368.
Drolet, G., Wade, T., Nichol, C.J., Maclellan, C., Levula, J., Porcar-Castell, A., et al., 2014. A temperature-controlled spectrometer system for continuous and unattended measurements of canopy spectral radiance and reflectance. Int. J. Remote Sens. 35 (5), 1769–1785.
Du, S., Liu, L., Liu, X., Hu, J., 2017. Response of canopy solar-induced chlorophyll fluorescence to the absorbed photosynthetically active radiation absorbed by chlorophyll. Remote Sens. 9, 911.
España, M., Baret, F., Aries, F., Andrieu, B., Chelle, Michaël, 1999. Radiative transfer sensitivity to the accuracy of canopy structure description. the case of a maize canopy. Agronomie 19 (3–4), 241–254.
Field, C.B., Randerson, J.T., Malmström, C.M., 1995. Global net primary production: combining ecology and remote sensing. Remote Sens. Environ. 51, 74–88.
Frankenberg, C., Fisher, J.B., Worden, J., Badgley, G., Saatchi, S.S., Lee, J., Toon, G.C., Butz, A., Jung, M., Kuze, A., Yokota, T., 2011. New global observations of the terrestrial carbon cycle from GOSAT: patterns of plant fluorescence with gross primary productivity. Geophys. Res. Lett. 38, 351–365.
Frankenberg, C., O'Dell, C., Berry, J., Guanter, L., Joiner, J., Köhler, P., Pollock, R., Taylor, T.E., 2014. Prospects for chlorophyll fluorescence remote sensing from the Orbiting Carbon Observatory-2. Remote Sens. Environ. 147, 1–12.
Frankenberg, C., O'Dell, C., Guanter, L., McDuffie, J., 2012. Remote sensing of near-infrared chlorophyll fluorescence from space in scattering atmospheres: implications for its retrieval and interferences with atmospheric CO_2 retrievals. Atmospheric Measurement Techniques 5, 2081–2094.
Frankenberg, C., Berry, J.K., 2018. Solar induced chlorophyll fluorescence: origins, relation to photosynthesis and retrieval. In: Liang, Shunlin (Ed.), Comprehensive Remote Sensing. vol. 2018. Elsevier, 9780128032213, pp. 143–162.
Goulas, Y., Fournier, A., Daumard, F., Champagne, S., Ounis, A., Marloie, O., Moya, I., 2017. Gross primary production of a wheat canopy relates stronger to far red than to red solar-induced chlorophyll fluorescence. Remote Sens. 9, 97.
Gowik, U., Westhoff, P., 2011. The Path from C3 to C4 photosynthesis. Plant Physiol. 155, 56–63.
Gu, L., Baldocchi, D., Verma, S.B., Black, T.A., Vesala, T., Falge, E.M., et al., 2002. Advantages of diffuse radiation for terrestrial ecosystem productivity. Journal of Geophysical Research Atmospheres 107 (D6) ACL-1-ACL 2-23.
Gu, L., Fuentes, J.D., Shugart, H.H., Staebler, R.M., Black, T.A., 1999. Responses of net ecosystem exchanges of carbon dioxide to changes in cloudiness: results from two north american deciduous forests. Journal of *Geophysical Research Atmospheres* 104 (D24), 31421–31434.
Gu, L., Wood, J.D., Chang, C.Y.-Y., Sun, Y., Riggs, J.S., 2018. Advancing terrestrial

ecosystem science with a novel automated measurement system for sun-induced chlorophyll fluorescence for integration with eddy covariance flux networks. J. Geophys. Res.: Biogeosciences 123.
Guanter, L., Frankenberg, C., Dudhia, A., Lewis, P.E., Gómez-Dans, J., Kuze, A., Suto, H., Grainger, R.G., 2012. Retrieval and global assessment of terrestrial chlorophyll fluorescence from GOSAT space measurements. Remote Sens. Environ. 121, 236–251.
Guanter, L., Zhang, Y., Jung, M., Joiner, J., Voigt, M., Berry, J.A., Frankenberg, C., Huete, A.R., Zarco-Tejada, P., Lee, J.E., Moran, M.S., Ponce-Campos, G., Beer, C., Camps-Valls, G., Buchmann, N., Gianelle, D., Klumpp, K., Cescatti, A., Baker, J.M., Griffis, T.J., 2014. Global and time-resolved monitoring of crop photosynthesis with chlorophyll fluorescence. Proc. Natl. Acad. Sci. 111, E1327–E1333.
Haboudane, D., Miller, J.R., Pattey, E., et al., 2004. Hyperspectral vegetation indices and novel algorithms for predicting green LAI of crop canopies: modeling and validation in the context of precision agriculture[J]. Remote Sens. Environ. 90 (3), 337–352.
Hu, J., Liu, L., Guo, J., Du, S., Liu, X., 2018. Upscaling solar-induced chlorophyll fluorescence from an instantaneous to daily scale gives an improved estimation of the gross primary productivity. Remote Sens. 10, 1663.
Joiner, J., Guanter, L., Lindstrot, R., Voigt, M., Vasilkov, A.P., Middleton, E.M., Huemmrich, K.F., Yoshida, Y., Frankenberg, C., 2013. Global monitoring of terrestrial chlorophyll fluorescence from moderate-spectral-resolution near-infrared satellite measurements: methodology, simulations, and application to GOME-2. Atmospheric Measurement Techniques 6, 2803–2823.
Joiner, J., Yoshida, Y., Vasilkov, A.P., Yoshida, Y., Corp, L.A., Middleton, E.M., 2011. First observations of global and seasonal terrestrial chlorophyll fluorescence from space. Biogeosciences 8, 637–651.
Kljun, N., Calanca, P., Rotach, M.W., Schmid, H.P., 2004. A simple parameterisation for flux footprint predictions. Boundary-Layer Meteorol. 112 (3), 503–523.
Kumar, R., Umanand, L., 2005. Estimation of global radiation using clearness index model for sizing photovoltaic system. Renew. Energy 30 (15), 2221–2233.
Lancashire, P., Bleiholder, H., Langeluddecke, P., Stauss, R., Asselt, T., Weber, E., et al., 1991. An uniform decimal code for growth stages of crops and weeds. Ann. Appl. Biol. 119 (3), 561–601.
Lara, M.V., Andreo, C.S., 2011. C4 plants adaptation to high levels of CO2 and to drought environments. In: Shanker, A. (Ed.), Abiotic Stress in Plants-Mechanisms and Adaptations. InTech, pp. 415–428.
Li, X., Xiao, J., He, B., 2018. Chlorophyll fluorescence observed by OCO-2 is strongly related to gross primary productivity estimated from flux towers in temperate forests. Remote Sens. Environ. 204, 659–671.
Liu, L., Guan, L., Liu, X., 2017. Directly estimating diurnal changes in GPP for C3 and C4 crops using far-red sun-induced chlorophyll fluorescence. Agric. For. Meteorol. 232, 1–9.
Liu, L., Liu, X., Wang, Z., Zhang, B., 2016. Measurement and analysis of bidirectional SIF emissions in wheat canopies. IEEE Trans. Geosci. Remote Sens. 54 (5), 2640–2651.
Liu, X., Guanter, L., Liu, L., Damm, A., Malenovský, Z., Rascher, U., et al., 2018. Downscaling of solar-induced chlorophyll fluorescence from canopy level to photosystem level using a random forest model. Remote Sens. Environ. 231. https://doi.org/10.1016/j.rse.2018.05.035.
Liu, X., Guo, J., Hu, J., Liu, L., 2019. Atmospheric correction for tower-based solar-induced chlorophyll fluorescence observations at O2-A band. Remote Sens. 11 (3), 355.
Magney, T.S., Bowling, D.R., Logan, B.A., Grossmann, K., Stutz, J., Blanken, P.D., Burns, S.P., Cheng, R., Garcia, M.A., Köhler, P., Lopez, S., Parazoo, N.C., Raczka, B., Schimel, D., Frankenberg, C., 2019. Mechanistic evidence for tracking the seasonality of photosynthesis with solar-induced fluorescence. Proc. Natl. Acad. Sci. 201900278.
Mazzoni, M., Meroni, M., Fortunato, C., Colombo, R., Verhoef, W., 2012. Retrieval of maize canopy fluorescence and reflectance by spectral fitting in the O2–A absorption band. Remote Sens. Environ. 124, 72–82.
Medlyn, B.E., 1998. Physiological basis of the light use efficiency model. TREE PHYSIOLOGY 18 (3), 167–176. https://doi.org/10.1093/treephys/18.3.167.
Meroni, M., Busetto, L., Colombo, R., Guanter, L., Moreno, J., Verhoef, W., 2010. Performance of spectral fitting methods for vegetation fluorescence quantification. Remote Sens. Environ. 114, 363–374.
Meroni, M., Colombo, R., 2006. Leaf level detection of solar induced chlorophyll fluorescence by means of a subnanometer resolution spectroradiometer. Remote Sens. Environ. 103, 438–448.
Miao, G., Guan, K., Yang, X., Bernacchi, C.J., Berry, J.A., DeLucia, E.H., Wu, J., Moore, C.E., Meacham, K., Cai, Y., Peng, B., Kimm, H., Masters, M.D., 2018. Sun-induced chlorophyll fluorescence, photosynthesis, and light use efficiency of a soybean field from seasonally continuous measurements. J. Geophys. Res.: Biogeosciences 123, 610–623.
Migliavacca, M., Perez-Priego, O., Rossini, M., El-Madany, T.S., Moreno, G., van der Tol, C., et al., 2017. Plant functional traits and canopy structure control the relationship between photosynthetic CO $_2$ uptake and far-red sun-induced fluorescence in a Mediterranean grassland under different nutrient availability. New Phytol. 214 (3), 1078–1091. https://doi.org/10.1111/nph.14437.
Monteith, J.L., 1972. Solar radiation and productivity in tropical ecosystems. J. Appl. Ecol. 9 (3), 747–766.
Porcar-Castell, A., Tyystjärvi, E., Atherton, J., van der Tol, C., Flexas, J., Pfündel, E.E., Moreno, J., Frankenberg, C., Berry, J.A., 2014. Linking chlorophyll a fluorescence to photosynthesis for remote sensing applications: mechanisms and challenges. J. Exp. Bot. 65, 4065–4095.
Qiu, B., Xue, Y., Fisher, J.B., Guo, W., Berry, J.A., Zhang, Y., 2018. Satellite chlorophyll fluorescence and soil moisture observations lead to advances in the predictive understanding of global terrestrial coupled carbon-water cycles. Glob. Biogeochem. Cycles 32, 360–375.
Rascher, U., Alonso, L., Burkart, A., Cilia, C., Cogliati, S., Colombo, R., Damm, A., Drusch, M., Guanter, L., Hanus, J., Hyvärinen, T., Julitta, T., Jussila, J., Kataja, K., Kokkalis, P., Kraft, S., Kraska, T., Matveeva, M., Moreno, J., Muller, O., Panigada, C., Pikl, M., Pinto, F., Prey, L., Pude, R., Rossini, M., Schickling, A., Schurr, U., Schüttemeyer, D., Verrelst, J., Zemek, F., 2015. Sun-induced fluorescence - a new probe of photosynthesis: first maps from the imaging spectrometer HyPlant. Glob. Chang. Biol. 21, 4673–4684.
Reichstein, M., Falge, E., Baldocchi, D., Papale, D., Aubinet, M., Berbigier, P., Bernhofer, C., Buchmann, N., Gilmanov, T., Granier, A., Grunwald, T., Havrankova, K., Ilvesniemi, H., Janous, D., Knohl, A., Laurila, T., Lohila, A., Loustau, D., Matteucci, G., Meyers, T., Miglietta, F., Ourcival, J., Pumpanen, J., Rambal, S., Rotenberg, E., Sanz, M., Tenhunen, J., Seufert, G., Vaccari, F., Vesala, T., Yakir, D., Valentini, R., 2005. On the separation of net ecosystem exchange into assimilation and ecosystem respiration: review and improved algorithm. Glob. Chang. Biol. 11, 1424–1439.
Rouse, J.W.J., Haas, R.H., Schell, J.A., Deering, D.W., 1973. Monitoring Vegetation Systems in the Great Plains with Erts, vol. 351. Nasa Special Publication, pp. 309.
Ryu, Y., Baldocchi, D.D., Kobayashi, H., van Ingen, C., Li, J., Black, T.A., Beringer, J., van Gorsel, E., Knohl, A., Law, B.E., Roupsard, O., 2011. Integration of MODIS land and atmosphere products with a coupled-process model to estimate gross primary productivity and evapotranspiration from 1 km to global scales. Glob. Biogeochem. Cycles 25 (GB4017).
Sage, R.F., Monson, R.K., 1999. C_4 Plant Biology Academic, San Diego, Calif.
Sage, R.F., Zhu, X.G., 2011. Exploiting the engine of C4 photosynthesis. J. Exp. Bot. 62 (9), 2989–3000. https://doi.org/10.1093/jxb/err179. May 2011.
Stewart, D.W., Costa, C., Dwyer, L.M., Smith, D.L., Hamilton, R.I., Ma, B.L., 2003. Canopy structure, light interception, and photosynthesis in maize. Agron. J. 95 (6), 1465.
Still, C.J., Berry, J.A., Collatz, G.J., Defries, R.S., 2003. Global distribution of c 3 and c 4 vegetation: carbon cycle implications. Glob. Biogeochem. Cycles 17 (1) 6-1-6-14.
Still, C.J., Riley, W.J., Biraud, S.C., Noone, D.C., Buenning, N.H., Randerson, J.T., et al., 2009. Influence of clouds and diffuse radiation on ecosystem-atmosphere co 2 and co 18 o exchanges. Journal of Geophysical Research Biogeosciences 114 (G1).
Sun, Y., Frankenberg, C., Jung, M., Joiner, J., Guanter, L., Köhler, P., Magney, T., 2018. Overview of solar-induced chlorophyll fluorescence (SIF) from the orbiting carbon observatory-2: retrieval, cross-mission comparison, and global monitoring for GPP. Remote Sens. Environ. 209, 808–823.
Van der Tol, C., Berry, J., Campbell, P., Rascher, U., 2014. Models of fluorescence and photosynthesis for interpreting measurements of solar-induced chlorophyll fluorescence. J. Geophys. Res. Biogeosci. 119 (12), 2312–2327.
Verma, M., Schimel, D., Evans, B., Frankenberg, C., Beringer, J., Drewry, D.T., Magney, T., Marang, I., Hutley, L., Moore, C., Eldering, A., 2017. Effect of environmental conditions on the relationship between solar-induced fluorescence and gross primary productivity at an OzFlux grassland site. J. Geophys. Res.: Biogeosciences 122, 716–733.
Verrelst, J., Rivera, J.P., Van der Tol, C., Magnani, F., Mohammed, G., Moreno, J., 2015. Global sensitivity analysis of the SCOPE model: what drives simulated canopy-leaving sun-induced fluorescence? Remote Sens. Environ. 166, 8–21.
Verrelst, J., Van der Tol, C., Magnani, F., Sabater, N., Rivera, J.P., Mohammed, G., Moreno, J., 2016. Evaluating the predictive power of sun-induced chlorophyll fluorescence to estimate net photosynthesis of vegetation canopies: a SCOPE modeling study. Remote Sens. Environ. 176, 139–151.
Viña, A., Gitelson, A.A., 2005. New developments in the remote estimation of the fraction of absorbed photosynthetically active radiation in crops. Geophys. Res. Lett. 32.
Wagle, P., Zhang, Y., Jin, C., Xiao, X., 2016. Comparison of solar-induced chlorophyll fluorescence, light-use efficiency, and process-based GPP models in maize. Ecol. Appl. 26, 1211–1222.
Weiss, M., Baret, F., Smith, G.J., Jonckheere, I., Coppin, P., 2003. Review of methods for in situ leaf area index (lai) determination: part ii. estimation of lai, errors and sampling. Agric. For. Meteorol. 121 (1–2), 0–53.
Wood, J.D., Griffis, T.J., Baker, J.M., Frankenberg, C., Verma, M., Yuen, K., 2017. Multiscale analyses of solar-induced fluorescence and gross primary production. Geophys. Res. Lett. 44, 533–541.
Wieneke, S., Ahrends, H., Damm, A., Pinto, F., Stadler, A., Rossini, M., Rascher, U., 2016. Airborne based spectroscopy of red and far-red sun-induced chlorophyll fluorescence: Implications for improved estimates of gross primary productivity. Remote Sens. Environ. 184, 654–667. https://doi.org/10.1016/j.rse.2016.07.025.
Wieneke, S., Burkart, A., Cendrero-Mateo, M.P., Julitta, T., Rossini, M., Schickling, A., et al., 2018. Linking photosynthesis and sun-induced fluorescence at sub-daily to seasonal scales. Remote Sens. Environ. 219, 247–258.
Yang, K., Ryu, Y., Dechant, B., Berry, J.A., Hwang, Y., Jiang, C., Kang, M., Kim, J., Kimm, H., Kornfeld, A., Yang, X., 2018a. Sun-induced chlorophyll fluorescence is more strongly related to absorbed light than to photosynthesis at half-hourly resolution in a rice paddy. Remote Sens. Environ. 216, 658–673.
Yang, X., Shi, H., Stovall, A., Guan, K., Miao, G., Zhang, Y., Zhang, Y., Xiao, X., Ryu, Y., Lee, J., 2018c. FluoSpec 2—an automated field spectroscopy system to monitor canopy solar-induced fluorescence. Sensors 18, 2063.
Yang, X., Tang, J., Mustard, J.F., Lee, J., Rossini, M., Joiner, J., Munger, J.W., Kornfeld, A., Richardson, A.D., 2015. Solar-induced chlorophyll fluorescence that correlates with canopy photosynthesis on diurnal and seasonal scales in a temperate deciduous forest. Geophys. Res. Lett. 42, 2977–2987.
Yang, P., van der Tol, C., 2018b. Linking canopy scattering of far-red sun-induced chlorophyll fluorescence with reflectance. Remote Sens. Environ. 209, 456–467.
Yang, P., van der Tol, C., Verhoef, W., Damm, A., Schickling, A., Kraska, T., Muller, O., Rascher, U., 2018b. Using reflectance to explain vegetation biochemical and structural effects on sun-induced chlorophyll fluorescence. Remote Sens. Environ. 231https://doi.org/10.1016/j.rse.2018.11.039. 0034-4257.
Zarco-Tejada, P.J., Berni, J.A.J., Suárez, L., Sepulcre-Cantó, G., Morales, F., Miller, J.R., 2009. Imaging chlorophyll fluorescence with an airborne narrow-band multispectral camera for vegetation stress detection. Remote Sens. Environ. 113, 1262–1275.

Zarco-Tejada, P.J., Morales, A., Testi, L., Villalobos, F.J., 2013. Spatio-temporal patterns of chlorophyll fluorescence and physiological and structural indices acquired from hyperspectral imagery as compared with carbon fluxes measured with eddy covariance. Remote Sens. Environ. 133, 102–115.

Zeng, Y., Badgley, G., Dechant, B., Ryu, Y., Chen, M., Berry, J.A., 2019. A practical approach for estimating the escape ratio of near-infrared solar-induced chlorophyll fluorescence. Remote Sens. Environ. 232. https://doi.org/10.1016/j.rse.2019.05.028.

Zhang, Y., Guanter, L., Berry, J.A., van der Tol, C., Yang, X., Tang, J., Zhang, F., 2016. Model-based analysis of the relationship between sun-induced chlorophyll fluorescence and gross primary production for remote sensing applications. Remote Sens. Environ. 187, 145–155.

Zhang, Y., Xiao, X., Zhang, Y., Wolf, S., Zhou, S., Joiner, J., Guanter, L., Verma, M., Sun, Y., Yang, X., Paul-Limoges, E., Gough, C.M., Wohlfahrt, G., Gioli, B., van der Tol, C., Yann, N., Lund, M., de Grandcourt, A., 2018a. On the relationship between sub-daily instantaneous and daily total gross primary production: implications for interpreting satellite-based SIF retrievals. Remote Sens. Environ. 205, 276–289.

Zhang, Yao, Xiao, X., Wolf, S., Wu, J., Wu, X., Gioli, B., Cescatti, A., Van Der Tol, C., Zhou, S., Gough, C., Gentine, P., Zhang, Yongguang, Steinbrecher, R., Ardö, J., 2018b. Spatio-temporal convergence of maximum daily light-use efficiency based on radiation absorption by canopy chlorophyll. Geophys. Res. Lett. 3508–3519.

Zhao, M., Heinsch, F.A., Nemani, R.R., Running, S.W., 2005. Improvements of the MODIS terrestrial gross and net primary production global data set. Remote Sens. Environ. 95, 164–176.